Regenerative Therapy 26 (2024) 132–144

Contents lists available at ScienceDirect

Regenerative Therapy

journal homepage: http://www.elsevier.com/locate/reth

Original Article

Bioactive glass 1393 promotes angiogenesis and accelerates wound healing through ROS/P53/MMP9 signaling pathway

Xuenan Chen [a, b, 1], Xinyu Ran [a, 1], Xuebo Wei [a, 1], Lifei Zhu [c], Shaodong Chen [d], Zhiyong Liao [b, **], Ke Xu [a, b, *], Weidong Xia [a, ***]

[a] National Key Clinical Specialty(Wound Healing), Burn and Wound Healing Center, The First Affliated Hospital of Wenzhou Medical University, Wenzhou, China
[b] College of Life and Environmental Sciences, Wenzhou University, Zhejiang, China
[c] School of Pharmaceutical Sciences, Cixi Biomedical Research Institute, Wenzhou Medical University, Zhejiang, China
[d] Department of Orthopaedics, Lishui People's Hospital, Zhejiang, China

ARTICLE INFO

Article history:
Received 29 March 2024
Received in revised form
20 May 2024
Accepted 26 May 2024

Keywords:
Bioactive glass 1393
Angiogenesis
Wound healing
Endothelial cells

ABSTRACT

Compared to bioactive glass 45S5, bioactive glass 1393 has shown greater potential in activating tissue cells and promoting angiogenesis for bone repair. Nevertheless, the effect of bioactive glass 1393 in the context of wound healing remains extensively unexplored, and its mechanism in wound healing remains unclear. Considering that angiogenesis is a critical stage in wound healing, we hypothesize that bioactive glass 1393 may facilitate wound healing through the stimulation of angiogenesis. To validate this hypothesis and further explore the mechanisms underlying its pro-angiogenic effects, we investigated the impact of bioactive glass 1393 on wound healing angiogenesis through both *in vivo* and *in vitro* studies. The research demonstrated that bioactive glass 1393 accelerated wound healing by promoting the formation of granulation, deposition of collagen, and angiogenesis. The results of Western blot analysis and immunofluorescence staining revealed that bioactive glass 1393 up-regulated the expression of angiogenesis-related factors. Additionally, bioactive glass 1393 inhibited the expression of ROS and P53 to promote angiogenesis. Furthermore, bioactive glass 1393 stimulated angiogenesis through the P53 signaling pathway, as evidenced by P53 activation assays. Collectively, these findings indicate that bioactive glass 1393 accelerates wound healing by promoting angiogenesis via the ROS/P53/MMP9 signaling pathway.

1. Introduction

Since its development by Professor Larry Hench at the University of Florida in 1972, bioactive glass has garnered significant interest due to its unique bioactivity compared to other biomaterials, as well as its strong bond with human soft tissues and outstanding stability. In 1985, bioactive glass began to be used in clinical settings to repair bone, articular cartilage, skin, and vascular injuries [1–4]. Bioactive glasses 45S5 consist of basic components such as 45% SiO_2, 24.5% Na_2O, 24.5% CaO, and 6% P_2O_5, along with additional metallic elements may be added to increase their bioactivity. Our previous research group has found that bioactive glass 45S5 can inhibit endothelial cells (ECs) pyroptosis and promote wound healing in mice by activating gap junction protein 43 [5]. Bioactive glass 1393, a silicate-based biomaterial, is composed of 53% SiO_2, 20% CaO, 6% Na_2O, 4% P_2O_5, 12% K_2O, and 5% MgO. Compared to bioactive glass 45S5, bioactive glass 1393 exhibits an elevated concentration of SiO_2 and supplemental network modifiers, such as MgO and K_2O [6,7]. Notably, Taimoor H conducted a study revealing that bioactive glass 1393 exhibited superior biological effects compared to conventional bioactive glass 45S5, specifically in promoting the proliferation and metabolism of human mesenchymal stromal cells (hMSCs) [6]. Similarly, Elke Kunisch reported

* Corresponding author.
** Corresponding author.
*** Corresponding author.
E-mail addresses: zyliao@wzu.edu.cn (Z. Liao), godxu1987@wzu.edu.cn (K. Xu), xiaweidong@wmu.edu.cn (W. Xia).

Peer review under responsibility of the Japanese Society for Regenerative Medicine.

[1] Xuenan Chen, Xinyu Ran and Xuebo Wei contributed equally to this work.

https://doi.org/10.1016/j.reth.2024.05.016

that bioactive glass 1393 exhibited higher cell proliferation and viability compared to bioactive glass 45S5, showing promising potential for bone regeneration and vascularization [8]. Although we have seen many promising findings with bioactive glass 1393, research on wound healing still appears relatively limited, which highlights the need for further research.

Bioactive glass 1393 exhibits a sustained release of K, Mg, Si, Na, Ca ions. Notably, recent studies have highlighted the potential of magnesium ions in promoting macrophage polarization and angiogenesis [9–11]. For instance, the release of Mg^{2+} and Si^{4+} from Mg-montmorillonite clay mineral has been shown to enhance revascularization in full-thickness skin wounds, stimulate epithelial regeneration, and facilitate collagen maturation in rats, thereby promoting wound healing [12]. Furthermore, Sharda et al. developed magnesium-loaded nanoparticles for wound healing, and the use of Mg-doped filipin membranes demonstrated improved wound healing activity across all experimental groups [13]. In addition, Our previous research group has found that phosphorus magnesium fibers release metal ions into wounds, which in turn regulate macrophage polarization and accelerate the wound healing process [9]. Based on these findings, it is reasonable to speculate that bioactive glass 1393 plays a pivotal role in the process of wound healing.

Vascularization stands as a vital process in wound healing, as it guarantees the transportation of oxygen and nutrient substance to the wound site while removing waste and carbon dioxide [14–16]. Angiogenesis, a key aspect of vascularization, involves the formation of ECs that create the intima and connect with smooth muscle cells and pericytes to constitute the perimembrane. The outer membrane consists of connective tissue, collagen, and fibers [17–19]. The establishment of a fully functional vascular system is indispensable for the effectiveness of wound healing. Throughout the angiogenic process, various factors related to angiogenesis play important roles [20,21]. Bioactive glass has been shown to stimulate endothelial or neighboring cells to secrete VEGF and eNOS, which improves ECs vascularization and angiogenesis [5,22]. Many studies have demonstrated that bioactive glass 1393 has good biocompatibility and cellular activity when in contact with ECs, and it has angiogenic capacity [23,24]. This indicates that bioactive glass 1393 has the potential to increase the expression of factors related to angiogenesis, which in turn may stimulate angiogenesis.

When skin injuries occur, they disrupt the vascular system in the surrounding tissue, leading to the accumulation of body fluids, inflammation, and hypoxia. In addition, the generation of reactive oxygen species (ROS) by various cells contributes to increased oxidative stress within the wounds [25,26]. Numerous studies have demonstrated that P53, as a target of ROS, is regulating the cellular response to DNA damage caused by ROS and apoptosis in the mitochondrial pathway [27–29]. Moreover, research has indicated that P53 regulates the expression of MMP9, a matrix metalloproteinase that has important functions in ECM degradation and wound healing regulation [30,31]. Therefore, it is hypothesized that bioactive glass1393 could influence angiogenesis and wound healing via the ROS/P53/MMP9 pathway.

In our investigation, our aim was to unveil the mechanisms behind the enhancement of wound healing facilitated by bioactive glass 1393. Specifically, we explored the impact of bioactive glass 1393 ion products on the rate of wound healing, the formation of granulation tissue, collagen deposition, and angiogenesis in an *in vivo* model, while assessing whether bioactive glass 1393 promotes angiogenesis through ROS/P53/MMP9 signaling in wound healing. Additionally, we assessed the protective effects of bioactive glass 1393 against ECs injury induced by lipopolysaccharide-adenosine triphosphate (LPS-ATP) through an *in vitro* model.

2. Materials and methods

2.1. Preparation of bioactive glass 1393 and 45S5

Bioactive glass 1393 was prepared by Hebei Yougu Biotechnology Co., following the previously reported method [32]. In brief, pure anhydrous silicic acid, sodium carbonate, potassium carbonate, sodium dihydrogen phosphate (all four of the above were provided by Riedel de Haen) were melted alongside magnesium carbonate and calcium carbonate (both supplied by Lachner) at 1400 °C in a platinum crucible for 2 h. The reaction was then quenched by rapidly cooling the samples in water. Subsequently, the bioactive glass was pre-ground using a jaw crusher (BB51, Retsch) and further ground to achieve the desired particle size in a planetary mill (PM100, Retsch) utilizing ZrO2 jars and ZrO2 grinding balls (Ø5 mm), both acquired from Retsch. Finally, the glass was filtered through a sieve for further use. bioactive glass 45S5 was purchased from Hebei Yougu Biotechnology Co.

2.2. Characterization of bioactive glass 1393

The ultrastructure surface of the bioactive glass was detected via scanning electron microscopy (SEM) (Hitachi, Japan). Subsequently, the functional groups on the surface of the samples were analyzed using Fourier Transform Infrared Spectrometer (FTIR) (Impact 420 Nicolet, Thermo Scientific). Furthermore, 1 g of bioactive glass 1393 was dissolved in 5 mL of pure water, and the resultant solution was left to immerse for 24 h. Afterward, the supernatant was collected and filtered through a 0.22 μm filter. Subsequently, inductively coupled plasma atomic emission spectrometry (ICP-OES 730, Agilent, USA) was employed to measure the amounts of Si and Mg present in the ionic extract of bioactive glass 1393.

2.3. Laboratory animals and surgery

Male ICR mice, aged between 6 and 8 weeks, were supplied by Wenzhou University. All experimental procedures and protocols received approval from the Animal Care and Use Committee of Wenzhou University (WZU-2022-020). Abbreviation explanation: The mice were anesthetized, and their dorsal hair was shaved to establish wound models [33]. Concentric fluoroelastomer washers were then fixed to both sides of their vertebrae using 5-0 sutures. Two circular full-thickness skin wound models were created using scissors. The washers possessed an inner diameter measuring 0.8 cm, an outer diameter measuring 1.6 cm, and a thickness measuring 0.05 cm. To prevent any scratching or chewing, the exposed skin was covered with a transparent dressing (3 M Health Care, Germany), and subsequently secured with an elastic bandage. The experimental cohort was then divided into two groups: Wound +45S5 group and Wound +1393 group. About 4 mg/cm^2 of bioactive glass 45S5 powder was administered to the wound in the former group, while the same concentration of bioactive glass 1393 powder was applied to the latter group. As a control, the negative control group (wound group) was only treated with injury. Wound healing was observed on postoperative days 0, 3, 6, 9, 12, and 15, respectively, and the degree of wound closure was quantified using Image J software. On postoperative days 7 and 14, mice were sacrificed and trauma tissues were harvested. Nutlin-3a (GC10470) was administered to activate P53. To explore the impact of P53 on trauma healing, mice were randomly assigned to the wound and Nutlin-3a group and the Nutlin-3a+1393 group. Nutlin-3a was administered intraperitoneally at a daily dose of 5 mg $kg^{-1}\cdot day^{-1}$.

2.4. Western blot

Proteins were extracted from tissues or cells using a RIPA lysate mixed with protease inhibitors and PMSF in proportional amounts, and all the aforementioned reagents were procured from Beyotime, China. After a 15-min centrifugation at 12,000 rpm and 4 °C, the supernatant was gathered, and the quantification of protein was performed. Subsequently, the proteins underwent separation via SDS-PAGE gel electrophoresis and then transferred onto PVDF (BioRad, USA). Following sealing with 5% low-fat milk for 2 h at room temperature, the membrane was exposed to the primary antibody overnight at 4 °C. The next day, the membranes were rinsed with TBST and subsequently exposed to horseradish peroxidase-labeled secondary antibody (Beyotime, China) for 2 h at room temperature. Detection of the blots was done using an enhanced chemiluminescence detection kit (Bio-Rad, USA). Image capture was executed with the ChemiDocXRS + imaging system (Bio-Rad, USA), Protein bands underwent quantitatively analyzed with Image J software. The study employed the following primary antibodies: CD31 (ab281583, Abcam), Ve-cadherin (ab205336, Abcam), NG2 (37–2700, USA), eNOS (27,120-1-AP, Proteintech), VEGF (19,003-1-AP, Proteintech), P53 (ab26, Abcam), MMP9 (ab283575, Abcam), and GAPDH (6004-1-lg, Proteintech).

2.5. Histological analysis and immunostaining

Fresh tissue samples underwent fixation in 4% paraformaldehyde for 24 h, followed by a 4-h wash with running water. The fixed samples were then dehydrated using a series of ethanol gradients (70%, 80%, 95%, 100%), followed by embedding in paraffin. The paraffin-embedded samples were secured onto a microtome and sliced continuously to obtain 5 μm-thick sections. The sections were carefully mounted on slides, and Hematoxylin and Eosin (H&E) staining as well as Masson trichrome staining were conducted following the instructions provided by the staining kits purchased from Beyotime, China. The glass slides were sealed using neutral glue (Beyotime, China). Finally, the microscope (Leica Camera, Germany) was used to observe the tissue structure of the wound. For immunostaining of the tissue samples, the sections were deparaffinized using xylene, followed by rehydration through an ethanol gradient, and then were subjected to 15 min of treatment with 3% H_2O_2. Following antigen extraction using citric acid under high temperature and pressure, the sections were blocked with 5% BSA at 37 °C for 30 min before overnight incubation with the primary antibody at 4 °C. Primary polyclonal antibodies, including anti-Ki67 (27,309-1-AP, Proteintech), CD31 (ab281583, Abcam), NG2 (37–2700, ThermoFisher), and P53 (ab26, Abcam). The following day, the slides underwent washing with PBST and were then incubated with fluorescently labeled secondary antibodies for 2 h at 37 °C. Following this, the nuclei were stained using an antifluorescence quenching agent containing DAPI (Beyotime, China). Post-staining, the images were captured through the FV3000 laser confocal scanning microscope (Olympus Corporation, Japan).

2.6. Evaluation of blood flow in the wound area

Seven days post-surgery, a laser Doppler instrument (MoorLDI-2, Moor Instruments Limited, UK) was utilized to evaluate the reconstruction of the microvascular network in the wounds of mouse back. The blood flow and outcomes were detected vua the MoorLDI Review software.

2.7. Transmission electron microscopy (TEM)

To study the collagen fiber distribution, 1 × 1 × 1 mm trabecular tissue samples were taken on day 14 after surgery. Next, they were submerged in a 2.5% glutaraldehyde solution (pH 7.3–7.4) for overnight fixation. Finally, the samples underwent fixation with a mixture of osmium tetroxide and potassium ferricyanide for 2 h at room temperature. Ultrathin sections with a 50 nm thickness were obtained using an ultrathin slicer (Leica UC7, Germany) after a process of alcohol gradient dehydration, resin infiltration, and embedding followed by polymerization. The sections underwent staining with uranyl acetate and lead citrate before being photographed with a tungsten TEM (JEOLJEM1200EX, Japan).

2.8. Cell culture and treatment

Human umbilical vein endothelial cells (HUVECs) were obtained from the National Stem Cell Transformation Resource Center (DFSC-EC-01). The cells were cultured in ECs medium containing 5% fetal bovine serum, 1% (v/v) penicillin/streptomycin, along with ECs growth additives at 37 °C with 5% CO_2. For the establishment of the *in vitro* injury model induced by LPS and adenosine triphosphate (ATP), HUVECs were seeded into 6-well or 96-well plates. The cells were cultured in serum-free medium and pre-treated with bioactive glass 1393 powder for 24 h. Subsequently, they were exposed to 1 μg/ml LPS for 6 h. This was followed by stimulation with 5 mM ATP for 30 min.

2.9. Detection of cell death

The study employed the Lactate Dehydrogenase (LDH) release assay (Yi Sheng, China). First, a 96-well plate was stimulated for 6 h. Following this, it was centrifuged at 400 g for 5 min. Once centrifugation was complete, 120 μL of the supernatant was extracted and 60 μL of the LDH assay solution was added to it. The mixture underwent incubation at room temperature for 30 min, protected from light with gentle shaking. Afterwards, the absorbance value at 490 nm was measured through an enzyme meter, and the LDH release amount was calculated using the formula: %LDH release = 100 × (corrected reading of test wells - corrected reading of untreated wells)/(corrected maximum LDH release control - corrected reading of untreated wells).

2.10. Detection of ROS levels

Following the completion of drug stimulation, each well of a six-well plate was supplemented with 10 μM 2,7-dichlorohydrofluorescein (DCFH-DA) (Beyotime, China). Then, the cells were incubated at 37 °C for 20 min. Afterward, they were washed with PBS to eliminate any unbound DCFH-DA. Examination of the six-well plates was conducted using an inverted fluorescence microscope (Leica, DM3000, Germany) to visualize positive signals, which appeared as green fluorescence. To measure ROS in tissue samples, dihydroethidium (DHE), a commonly used fluorescent probe for detecting superoxide anions, was utilized. The tissue sections were subjected to deparaffinization, rehydration, and antigen retrieval. Subsequently, the sections were incubated with Beyotime's DHE dye for 30 min. Subsequently, they were rinsed with PBS, the sections were stained with an anti-fluorescence quenching agent. Finally, the tissue samples were imaged by an FV3000 laser confocal scanning microscope (Olympus Corporation, Japan).

2.11. Data analysis

All experiments were independently replicated at least 3 times, and the data are expressed as mean ± standard error of mean (SEM). Statistical analysis was conducted employing SPSS software. Student's t-test was utilized for comparison between the two

groups, while the single-factor analysis of variance (Tukey) test was utilized for comparing among multiple groups. A *p*-value below 0.05 was deemed statistically significant.

3. Results

3.1. Synthesis and characterization of bioactive glass 1393

Fig. 1A depicts the detailed synthetic route of bioactive glass 1393, resulting in the formation of a white powdery solid. In order to observe the macroscopic structure of bioactive glass 1393, SEM was employed. As shown in Fig. 1B, most of the particles of the bioactive glass 1393 were in the size range of ~10 μm. The FTIR spectrum of bioactive glass 1393, shown in Fig. 1C, exhibited absorption peaks corresponding to the asymmetric stretching vibrations of the Si–O bonds. Notably, an absorption peak around 1038 cm^{-1} was detected, a characteristic feature of silicate glasses and vitreous silica with a higher SiO_2 content. Additionally, a Si-NBO (non-bridging oxygen) peak was detected at around 930 cm^{-1}, accompanied by an increased intensity of the bending mode of the Si–O band at approximately 755 cm^{-1}. Another absorption peak appeared at approximately 475 cm^{-1}, indicating the presence of a silicon dioxide ring structure, which is a typical feature of silica ring structures. These findings align with those reported by Alexander Hoppe et al. regarding the characteristic peaks of bioactive glass 1393 [32]. We next measured the ion release from the bioactive glass 1393 extract using ICP-OES, and as shown in Fig. 1D, Si ions and Mg ions were detected in the leachate. As a result, the bioactive glass 1393 can release Mg and Si ions to function *in vivo*.

3.2. Bioactive glass 1393 promoted wound healing in vivo

To compare the wound healing effects of bioactive glass 1393 and 45S5, we established a full-thickness skin wound model in mice, as illustrated in Fig. 2A. Wound healing observations were made on postoperative days 0, 3, 6, 9, 12, and 15 for the Wound group, Wound+45S5 group, and Wound+1393 group (Fig. 2B). The application of both bioactive glass 45S5 and 1393 significantly reduced the wound area. Importantly, the bioactive glass 1393 treatment group exhibited a notably faster healing rate compared to the bioactive glass 45S5 treatment group. To provide a clear visualization of the healing process, the dynamic progression of wound healing was meticulously monitored. Wound sizes were recorded and color-coded for both groups on days 0, 3, 6, 9, 12, and 15, respectively (Fig. 2C). Next, we measured the area of the wound that remained unhealed at different time points for each group, as depicted in Fig. 2D. The group treated with the bioactive glass 1393 exhibited a considerably higher wound healing rate than the bioactive glass 45S5 treatment group on postoperative day 9, and the wound was nearly fully closed by postoperative day 15. Our results provide evidence that the bioactive glass 1393 outperforms the bioactive glass 45S5 and contributes significantly to wound healing.

3.3. Bioactive glass 1393 promoted skin tissue development, collagen deposition and cell proliferation in vivo

The evaluation of granulation tissue and collagen deposition is a critical measure for assessing the effects of drugs on skin wound repair [34,35]. Histological examination of the wound tissue was performed 14 days post-surgery using H&E staining and Masson staining (Fig. 3A). The results revealed that both bioactive glass 45S5 and 1393 exhibited a certain degree of reparative effect on the wound. Among them, the bioactive glass 1393 treatment group showed a more significant development of granulation tissue and higher levels of collagen deposition at the wound site in comparison to the bioactive glass 45S5 treatment group. Consistently, the length of unhealed wounds in the bioactive glass 1393 treatment group was shorter than that in the bioactive glass 45S5 treatment group, indicating a superior wound repair ability of the bioactive glass 1393 treatment (Fig. 3D). Furthermore, TEM was utilized to analyze the distribution of collagen fibers in the wounds on day 14, demonstrating enhanced improvement with the bioactive glass 1393 treatment group compared to the bioactive glass 45S5 treatment group (Fig. 3B). Additionally, the quantification of Ki67-positive cells, as depicted in Fig. 3C and E, revealed a significantly higher number of proliferating cells in the bioactive glass 1393 treatment group in comparison to the bioactive glass 45S5 treatment group. These observations indicate that the bioactive glass 1393 promotes cell proliferation in mice skin wounds, further supporting its beneficial effects on wound healing.

3.4. Bioactive glass 1393 promoted angiogenesis in mice

Considering the crucial role of ECs and angiogenesis-related factors in blood vessel formation, we hypothesized that bioactive glass 1393 might have an impact on ECs formation and the expression of angiogenesis-related factors (eNOS, VEGF). Based on this, Western blot analysis was conducted to assess the expression of ECs markers (CD31, Ve-cadherin) and angiogenesis-related factors (eNOS, VEGF). The results exhibited a notable elevation in the expression levels of CD31, Ve-cadherin, eNOS, and VEGF in the Wound+1393 group in comparison to the Wound group (Fig. 4A and B). To confirm the angiogenic status, co-staining of the pericyte marker NG2 and the ECs marker CD31 was performed. On the seventh day after the operation, there was a noteworthy increase in the quantity of NG2-positive cells in the bioactive glass 1393 treatment group compared to the wound group. The NG2-positive cells were found surrounding the ECs and adhering to CD31-labelled ECs in the bioactive glass 1393 treatment group. The bioactive glass 1393 treatment group exhibited a more intact vascular structure compared to the wound group, indicating that bioactive glass 1393 promotes the functional integrity of blood vessels (Fig. 4C). Furthermore, the formation of a newly developed vascular network and blood flow were evaluated at the wound site. The reconstruction of the microvascular network in the wound region was visualized utilizing LDBF, an indicator for blood flow, where a more intense red hue indicates higher blood flow. The bioactive glass 1393 treatment group demonstrated significantly higher blood flow intensity in comparison to the wound group (Fig. 4D and E), indicating that the bioactive glass 1393 facilitates angiogenesis.

3.5. Bioactive glass 1393 promotes angiogenesis and wound healing through the ROS/P53/MMP9 signaling pathway

To further evaluate the angiogenic properties of the bioactive glass 1393, tissue ROS levels were assessed. The staining results demonstrated a significant reduction in red fluorescence at the wound site in the bioactive glass 1393 treatment group in comparison to the wound group, suggesting the bioactive glass 1393's capability to decrease ROS levels (Fig. 5A and B). Additionally, Western blot was conducted to assess the expression of P53 and MMP9 (Fig. 5C and D). It was observed that P53 expression was upregulated in the wound group, whereas bioactive glass 1393 treatment resulted in decreased P53 expression and increased MMP9 expression. Furthermore, co-staining of P53 and CD31 revealed the expression of P53 protein on ECs, and the accumulation of P53-positive spots on those cells was notably decreased in the bioactive glass 1393 treatment group in comparison to the

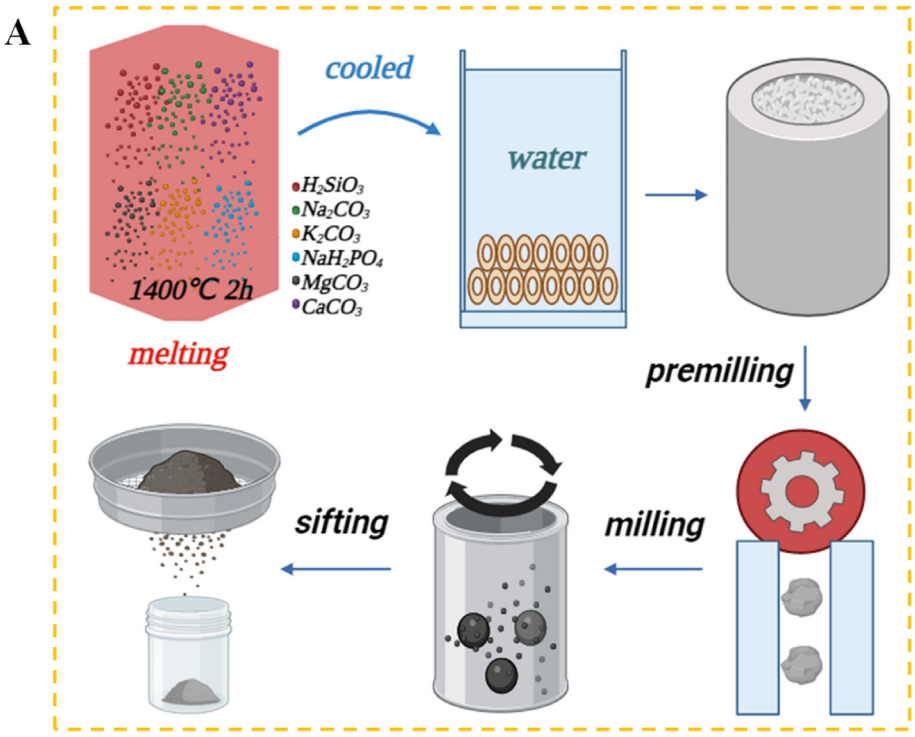

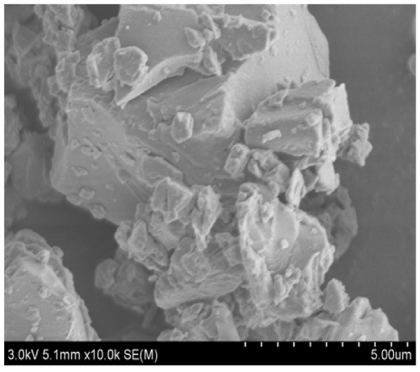

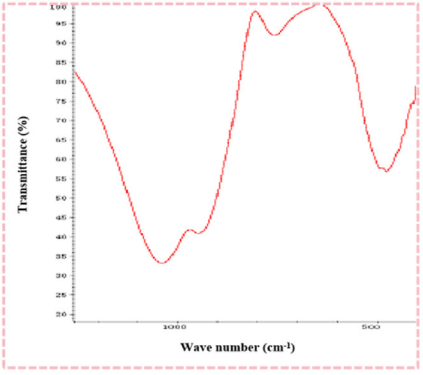

D

	Si (mg/L)	Mg (mg/L)
ddH_2O	undetected	undetected
ddH_2O+1393	9.7	2.7

Fig. 1. Synthesis and characterization of bioactive glass 1393. (A) Schematic diagram of the synthesis of bioactive glass 1393. (B) SEM image of bioactive glass 1393. Scale bar = 5 μm. (C) FTIR spectrum of bioactive glass 1393. (D) Concentration of ions in the extract of bioactive glass 1393.

wound group (Fig. 5E). Overall, these findings imply that bioactive glass 1393 can down-regulate ROS and P53 expression levels, thereby promoting MMP9 expression and angiogenesis.

3.6. Impact of Nutlin-3a on wound healing in mice

To further validate the pivotal role of the P53 signaling pathway in fostering angiogenesis by bioactive glass 1393, we examined the effects of the P53 activator Nutlin-3a on wound healing in mice, which increased P53 protein level [36–38]. Fig. 6A–C illustrated that the mice in the Wound+1393+Nutlin-3a group had a larger wound area in comparison to the Wound+1393 group. Further analysis revealed that beginning from the third day, the wound region in the Wound+1393 group exhibited a notably lower measurement when compared to the Wound+1393+Nutlin-3a group. Furthermore, the Western blot results outcomes showcased notably elevated expression of angiogenesis-related proteins (eNOS and VEGF) and marker proteins of ECs (CD31 and Ve-cadherin) in the

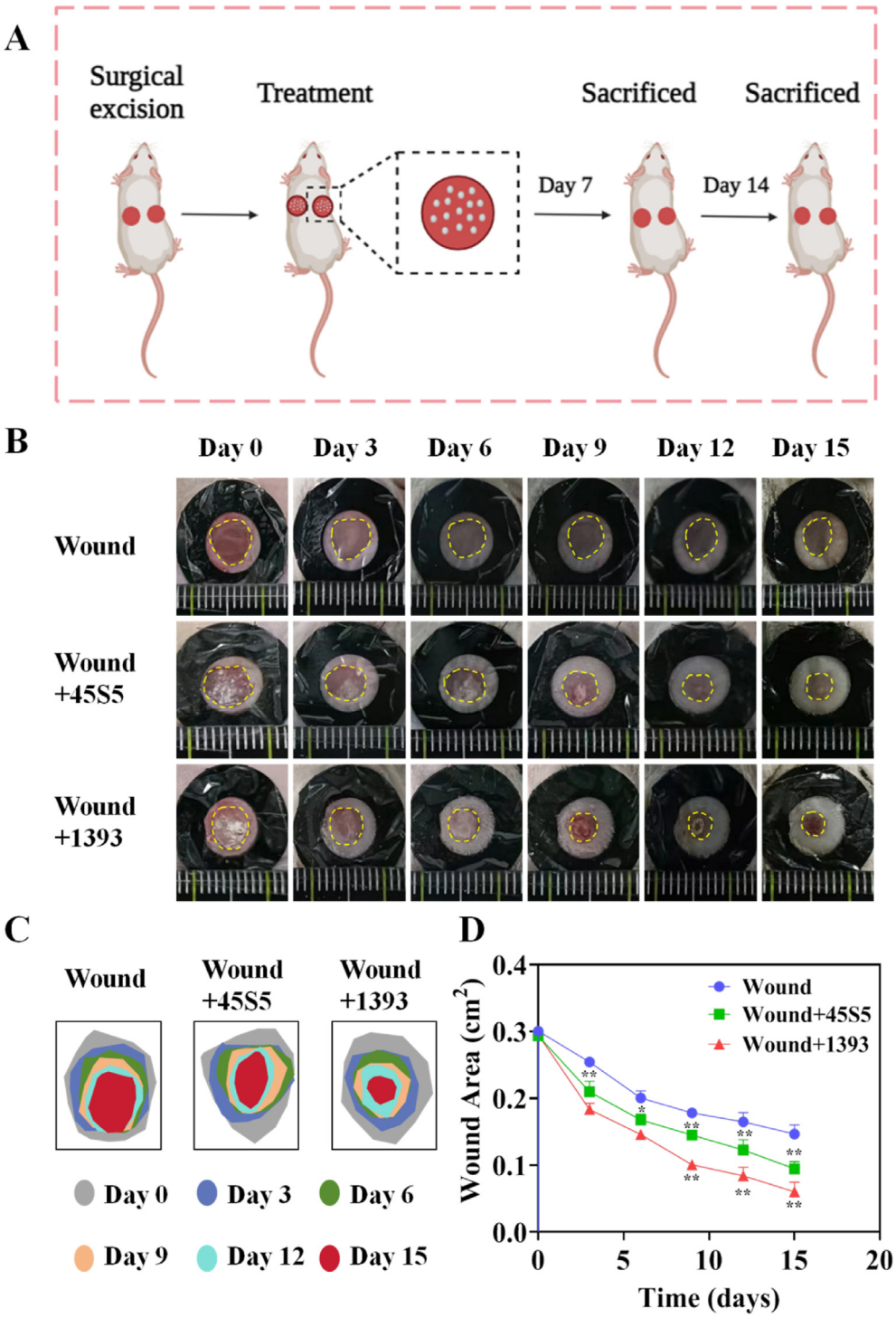

Fig. 2. The role of bioactive glass 1393 in promoting skin wound healing *in vivo*. (A) Schematic diagram of the animal experiment, two full-thickness excision wounds were made in each mouse. (B) Representative images of skin wound healing in mice in the Wound group, Wound+45S5 group and Wound+1393 group. Scale bar = 10 mm. (C) Schematic images of skin wound healing in mice in the Wound group, Wound+45S5 group and Wound+1393 group. (D) Statistics of wound area at different time points (0, 3, 6, 9, 12, and 15 days) for each of the above groups. n = 6, compared with the Wound group and Wound+45S5 group (*$P<0.05$, **$P < 0.01$).

Wound+1393 group in comparison to the Wound+1393+Nutlin-3a group. Additionally, in the Wound+1393 group, the levels of P53 proteins were significantly reduced in comparison to the Wound+1393+Nutlin-3a group, whereas the MMP9 protein levels were noticeably higher than those in the Wound+1393 group (Fig. 6D and E). These outcomes collectively demonstrate that the P53 activator influenced angiogenesis and wound healing in mice wounds, confirming that the bioactive glass 1393 promotes angiogenesis and wound healing through the P53/MMP9 signaling pathway.

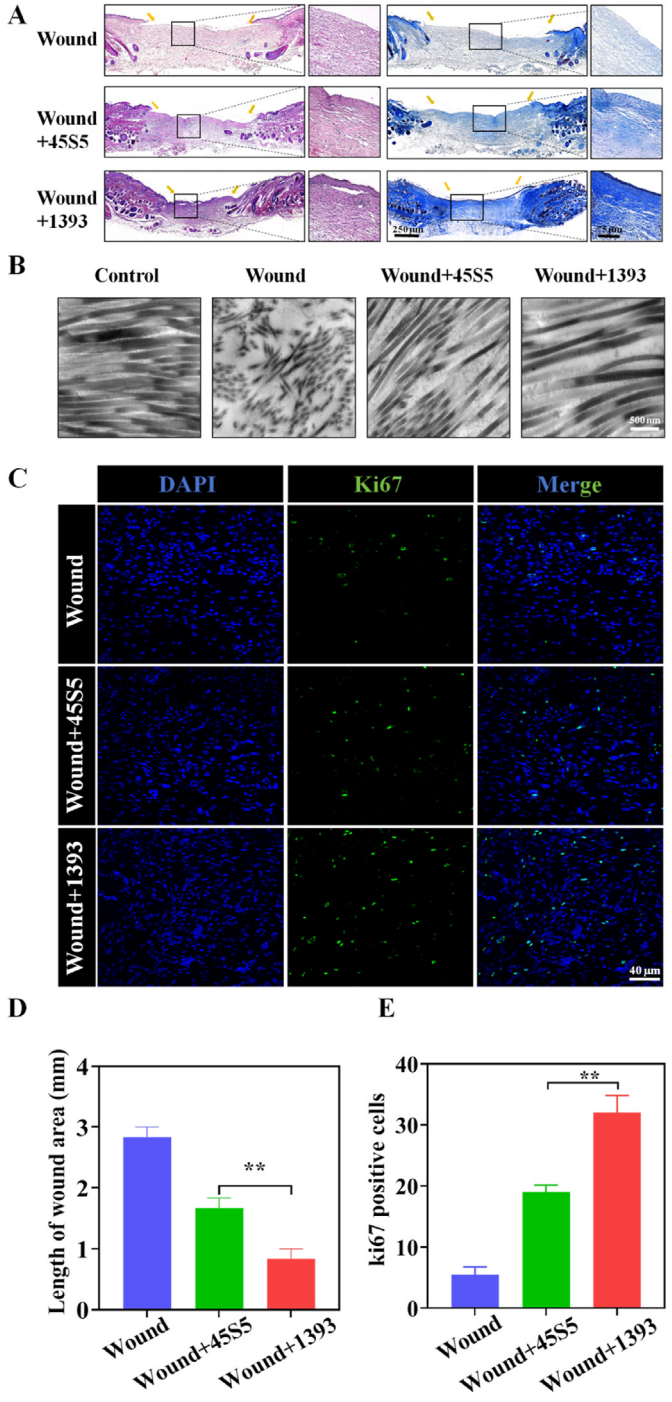

Fig. 3. Effectiveness of bioactive glass 1393 in promoting skin tissue development *in vivo*. (A) Wound tissue was taken on day 14 for histological analysis. Hematoxylin and eosin (H&E) staining was located on the left side, and Masson trichrome staining was located on the right side. Scale bar: low magnification is 250 μm, high magnification is 75 μm (B) Distribution of collagen fibers in each group of wounds on day 14 was observed by transmission electron microscopy. Scale bar = 500 nm (C, E) Ki67 fluorescence staining and quantitative analysis of the number of Ki67-positive cells. Scale bar = 40 μm, n = 6, compared with the Wound+45S5 group (**$P < 0.01$) (D) Wound length was evaluated by H&E staining images to assess wound healing, n = 3, compared with the Wound+45S5 group (**$P < 0.01$).

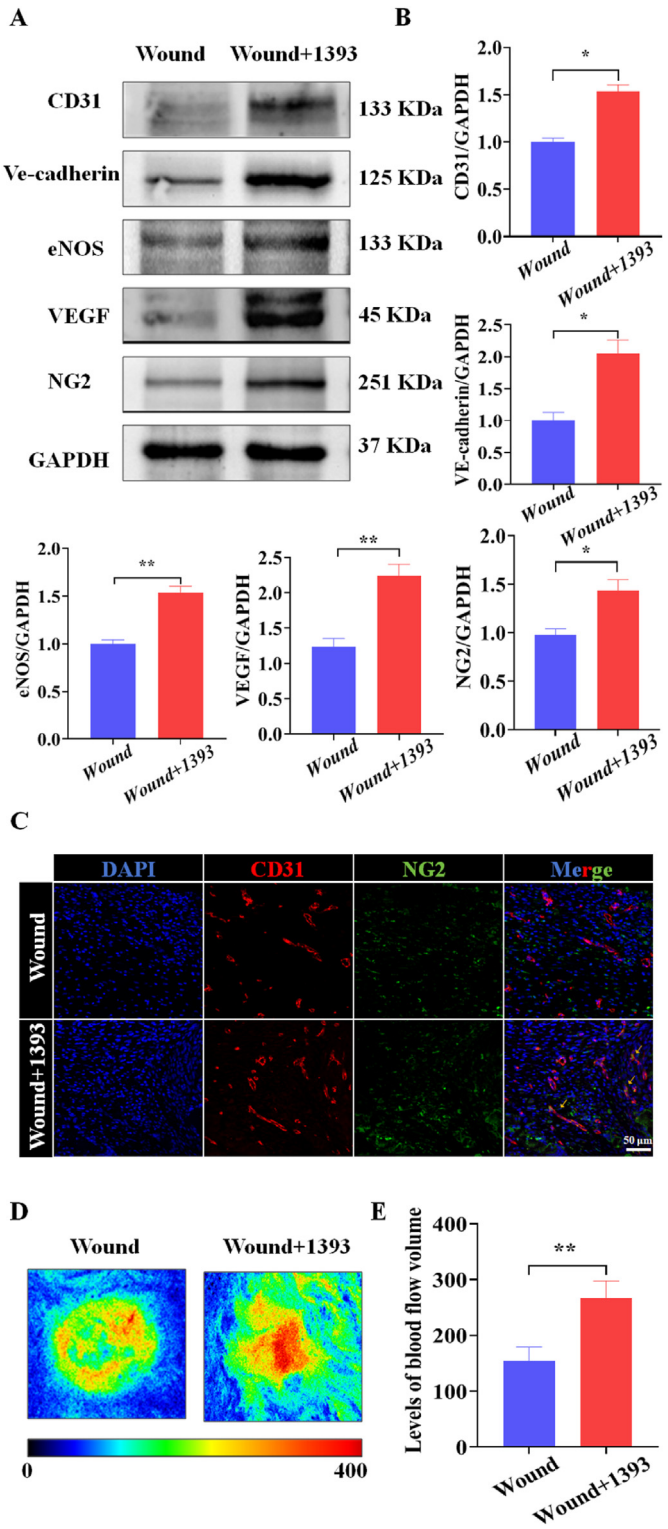

Fig. 4. Bioactive glass 1393 promotes angiogenesis *in vivo*. (A, B) Expression and quantification of angiogenesis-related proteins in each group on postoperative day 7, n = 3, compared with the Wound group (*$P<0.05$, **$P<0.01$). (C) Double-immunofluorescence staining for CD31 and NG2 in the trabeculae of each group on postoperative day 7, n = 5, scale bar = 50 μm. Yellow arrows indicate NG2-positive pericyte attachment. (D) Subcutaneous blood flow was assessed using representative color laser Doppler images on postoperative day 7. (E) Quantitative data on the signal intensity of blood flow in the skin trauma in each group. n = 3, compared with the Wound group (**$P < 0.01$).

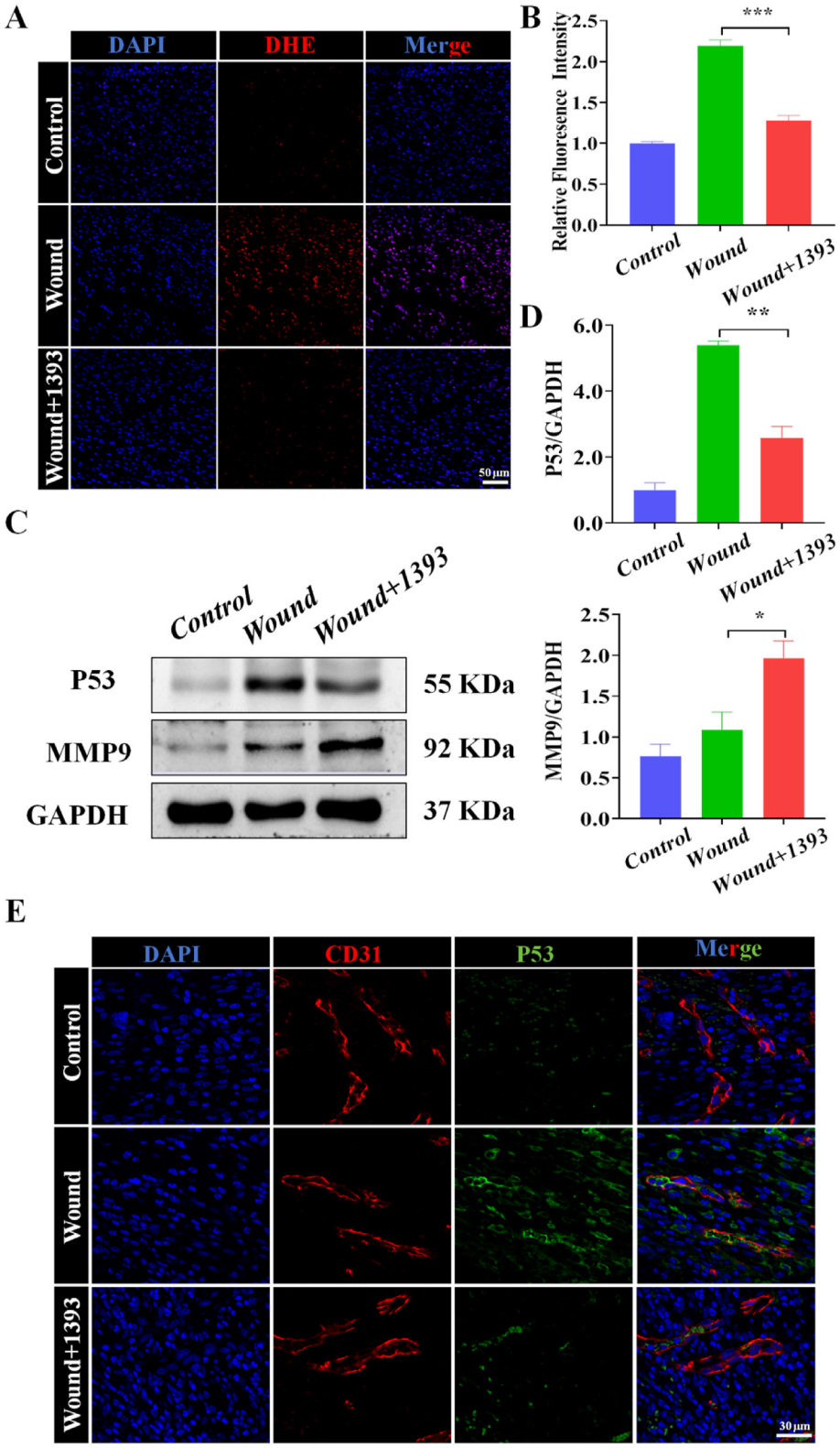

Fig. 5. Bioactive glass 1393 promotes angiogenesis through the ROS/P53/MMP9 signaling pathway. (A, B) ROS levels in the wound area under different treatments were measured by DHE. Scale bar = 50 μm, n = 6, compared with the Wound group (***$P < 0.001$) (C) On postoperative day 7, the expression levels of proteins related to the signaling pathway in the Control group, Wound group and the Wound+1393 group were determined by Western blot analysis. (D) Quantitative analysis of the expression levels of signaling pathway-related proteins in each group. n = 3, compared with the Wound group (*$P<0.05$, **$P < 0.01$). (E) Immunofluorescence staining was used to detect the expression and localization of P53 and CD31 in the trauma of mice on the 7th day after surgery. Scale bar = 30 μm, n = 4.

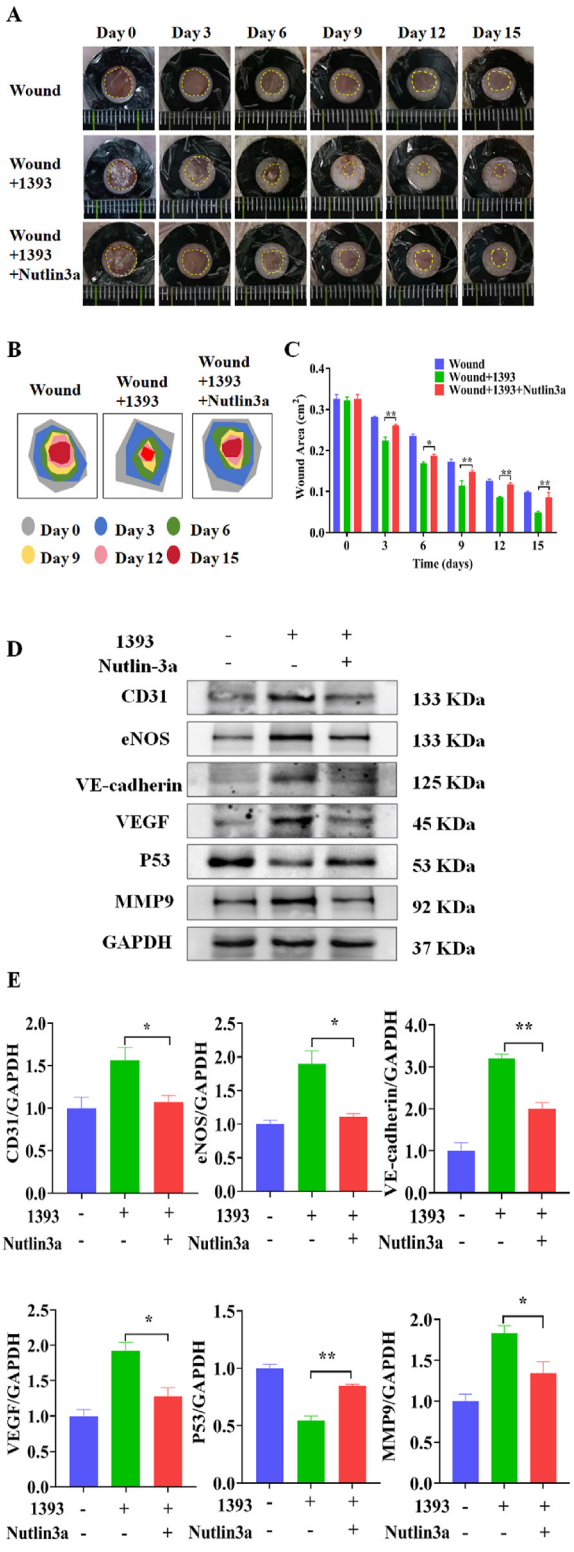

Fig. 6. Effect of Nutlin-3a on wound healing in mice (A) ICR male mice were randomly divided into Wound group, Wound + 1393 group and Wound + 1393+ Nutlin-3a group. Wound healing was monitored at different time points (days 0, 3, 6, 9, 12, and 15) in each group. (B) Schematic diagram of wound healing in mice at different time points in different treatment groups. (C) Statistics of wound area at different time points (0, 3, 6, 9, 12, 15 days) in each of the above groups. n = 6, compared with the Wound+1393 group (*$P < 0.05$, **$P < 0.01$) (D) Expression of angiogenesis-related proteins regulated by signaling pathways under the influence of Nutlin3a. (E) Statistical analysis of the expression of each protein between groups, n = 3, compared with the Wound+1393 group (*$P < 0.05$, **$P < 0.01$).

3.7. Bioactive glass 1393 promoted the secretion of angiogenesis-related factors in HUVECs

The *in vivo* experimental results have already demonstrated that bioactive glass 1393 enhances the expression of angiogenesis-related factors through the ROS/P53/MMP9 pathway. To further confirm this conclusion, we performed additional experiments using ECs in an *in vitro* setting. First, we assessed the cytotoxicity of bioactive glass 1393 b y diluting it to different concentrations (1/50, 1/100, 1/200, 1/500, 1/1000, 1/2000) using serum-free ECs culture medium. High concentrations of bioactive glass 1393 (1/50, 1/100, 1/200, 1/500) inhibited HUVEC proliferation, while low concentrations (1/1000, 1/2000) had minimal effect (Fig. 7A). Next, we used an LPS-ATP-induced ECs injury model and performed the LDH assay to determine the appropriate therapeutic concentration. The results showed that a dilution of 1/1000 of bioactive glass 1393 effectively rescued the LPS-ATP-induced injury in HUVECs (Fig. 7B). Further analysis using Western blot revealed that bioactive glass 1393 treatment up-regulated the expression of angiogenesis-related factors (eNOS, VEGF) in comparison to the LPS-ATP group (Fig. 7C and D), indicating that the bioactive glass 1393 had a stronger angiogenic capacity. Additionally, compared with the LPS-ATP group, the P53 expression was notably reduced in the bioactive glass 1393 treatment group, while the MMP9 expression was markedly elevated. These findings suggest that the bioactive glass 1393 promotes angiogenesis through the regulation of the ROS/P53/MMP9 pathway.

Moreover, DCFH-DA staining demonstrated a decrease in green fluorescence, indicating a reduction in oxidative stress in HUVECs treated with the bioactive glass 1393 (Fig. 7E). Overall, these *in vitro* experiments, coupled with the previous *in vivo* findings, provide further evidence supporting the role of the bioactive glass 1393 in enhancing angiogenesis-related factor expression through the ROS/P53/MMP9 pathway.

4. Discussion

The process of wound healing is complex, and angiogenesis plays a crucial role in the proliferative phase facilitating tissue repair. Numerous studies have underscored the substantial influence of bioactive glass 1393 ion products on stimulating genes related to cellular functions, particularly those involved in angiogenesis. It has been reported that bioactive glass 1393 can stimulate ECs or adjacent cells to secrete angiogenesis-related factors, thereby improving ECs vascularization and angiogenesis. Consequently, bioactive glass 1393 is considered to have the potential to promote wound healing by facilitating blood vessel formation within the wound. Nevertheless, the precise mechanism underlying this effect remains incompletely understood. Additionally, reducing ROS production can be beneficial for angiogenesis, which is a critical factor in the wound microenvironment. Given that P53 influences various cell types, there appears to be a significant correlation between ROS and P53. However, it remains unclear whether bioactive glass 1393 can modulate cellular behavior in wound healing by targeting P53. This study establishes that bioactive glass 1393 not only boosts the expression of factors related to angiogenesis in ECs but also impacts ROS production and the expression of P53 and MMP9. Consequently, it promotes vascular neogenesis both *in vitro* and *in vivo*, ultimately impacting the wound healing process (Fig. 8).

In recent years, metal cations have gained popularity in wound healing [39,40]. Our laboratory research has found that phosphorus magnesium fiber can activate TRPM7 channels, allowing magnesium ions to flow in and promote macrophage polarization to improve the wound microenvironment. Sodium and potassium

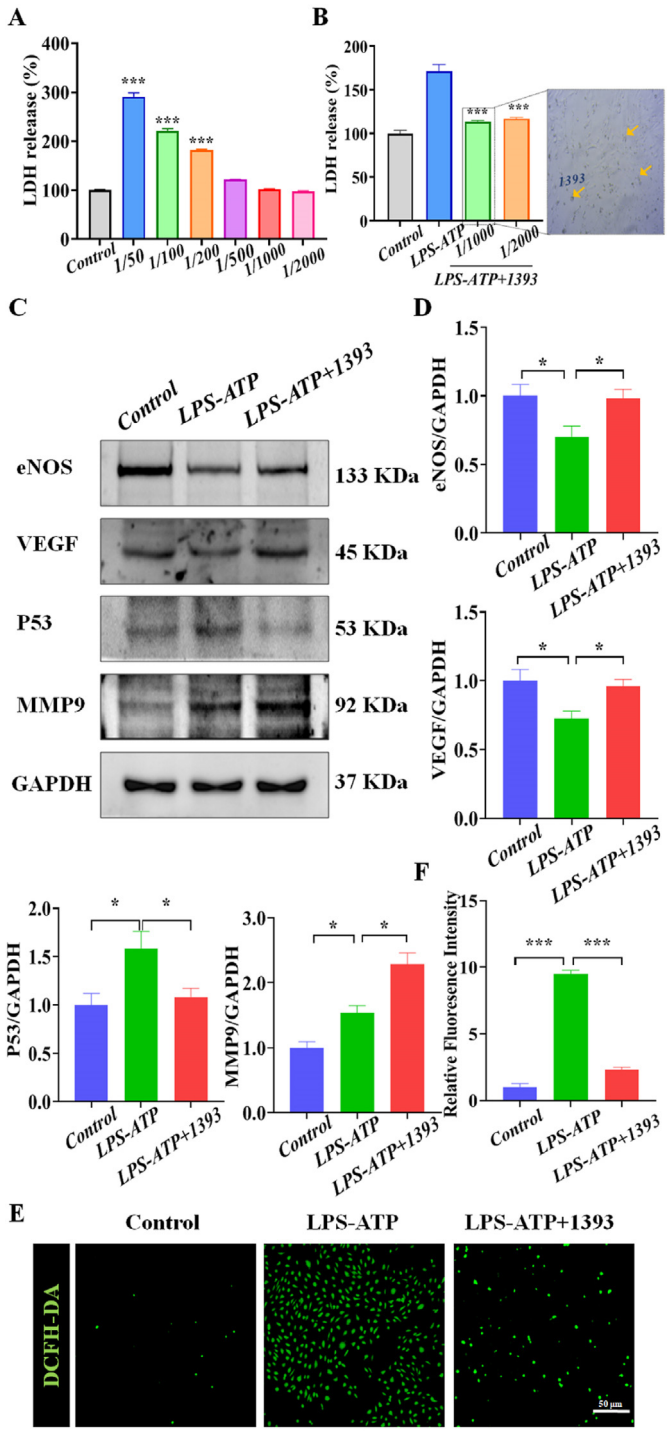

Fig. 7. Bioactive glass 1393 promotes secretion of angiogenesis-related factors in HUVECs. (A) LDH release in HUVECS treated with different concentrations of bioactive glass 1393 powder diluted at 1/50–1/2000, n = 6, compared with the control group (***$P<0.001$) (B) LDH release in HUVECS treated with LPS-ATP plus different concentrations of bioactive glass 1393 was assayed. Yellow arrows demonstrate the presence of bioactive glass particles, n = 6, compared with the LPS-ATP group (***$P < 0.001$) (C) Protein expression levels of P53, MMP9, eNOS, and VEGF in HUVECs were detected through Western blotting after being stimulated by treatment of LPS-ATP with 1/1000 BG (D) Quantitative analysis of angiogenesis-related protein expression levels in each group, n = 3 (*$P < 0.05$) (E, F) Levels of ROS in HUVECS were detected using DCFH-DA staining. Scale bar = 50 μm, n = 6 (***$P < 0.001$).

ions did not affect macrophage polarization [9]. Additionally, in this study, SEM was employed to analyze the particle size of bioactive glass 1393 and 45S5. Firstly, the potential impact of glass particle size on cell viability was ruled out. Secondly, the study showed that bioactive glass 1393 released a higher amount of magnesium ions compared to 45S5, as detected by ICP-OES, indicating the bioactive effects of bioactive glass 1393 through ion release. Moreover, granulation and collagen deposition are widely recognized as important factors in wound healing, providing a favorable environment for the growth of new blood vessels, and the ordered and dense arrangement of collagen supports the functional recovery of the skin [41–43]. The study implemented bioactive glass 1393 and 45S5 in a mouse model of injury and found that the bioactive glass 1393 treatment group actually promoted granulation, collagen deposition, collagen fiber alignment, and cell proliferation, thereby accelerating wound healing (Figs. 2 and 3). To summarize, bioactive glass 1393 treatment is more effective in wound healing than bioactive glass 45S5 treatment, possibly due to magnesium ion release, but further research is required.

Angiogenesis and the establishment of a functional vascular network are crucial for the process of wound healing [44]. The dynamic changes in the vascular system during wound healing involve angiogenesis, vascular maturation, and regression. The maturation of newly formed blood vessels heavily relies on the coordinated interaction between vascular ECs and perivascular cells [45]. During the initial stages of angiogenesis, perivascular cells are recruited from pre-existing vessels and contribute to blood vessel growth by degrading the extracellular matrix and releasing vascular growth factors. As blood vessel development progresses, perivascular cells migrate towards the periphery of the endothelium, providing structural stability and support. In this investigation, we noted a substantial rise in the formation of new blood vessels in the wounds of the group treated with bioactive glass 1393 on the seventh day after surgery (Fig. 4). Furthermore, NG2 is a well-known marker for perivascular cells in the skin [46–49]. The number of NG2-labeled cells surrounding the blood vessels increased and a significant improvement in vascularization was observed as the skin regenerated following injury. On the other hand, laser doppler imaging of the wound reveals that the group treated with bioactive glass 1393 had a higher wound blood flow compared to the wound group. This implies that bioactive glass 1393 not only enhances blood vessel formation but also expedites the development of functional blood vessels. eNOS and VEGF are crucial regulators of endothelial function and play a vital role in angiogenesis [22,50,51]. Studies have shown that VEGF, which is released immediately after an injury, promotes the proliferation and migration of vascular ECs, elevates vascular permeability, and induces the differentiation of ECs into capillaries [20]. eNOS has been recognized as a key player in angiogenic signaling during skin wound healing. Studies conducted in mouse models of ischemia have demonstrated that the genetic deletion of eNOS results in impaired angiogenesis [52]. In addition, two endothelial junction proteins have been used as endothelial markers in a large number of reports: CD31 and vascular endothelial calreticulin (VE-Cad) to detect vessel growth [53–55]. It has been reported that CD44 modulates cell proliferation and specific caspase-mediated apoptosis through the Hippo pathway by controlling the CD31 and VE-cadherin expression [56]. The experiments conducted both *in vivo* and *in vitro* in our study consistently demonstrate that bioactive glass 1393 induces the upregulation of angiogenesis-related factors (VEGF and eNOS) and endothelial markers (CD31, VE-cadherin). Collectively, these findings suggest that bioactive glass 1393 has the potential to promote angiogenesis. However, further investigations are required to elucidate the underlying mechanism.

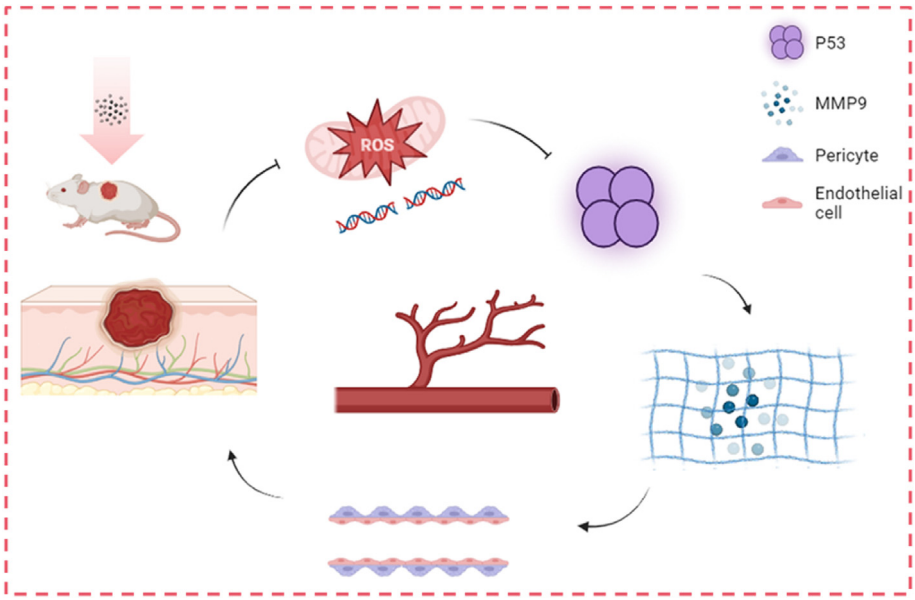

Fig. 8. Bioactive glass 1393 promotes wound healing by regulating the ROS/P53/MMP9 signaling pathway and promoting angiogenesis. Upon contact with wound body fluids, it diminishes oxidative stress levels in the wound, inhibiting P53 activation, and upregulating MMP9 protein levels to stimulate blood vessel maturation and formation, thereby accelerating wound healing.

Elevated intracellularly induced levels of ROS in the trauma microenvironment are believed to be the primary signal responsible for DNA damage. Free radicals bind to DNA, changing its physical or chemical state and causing DNA breaks, while DNA damage-induced P53 may arrest the cell cycle and induce apoptosis [57–59]. Qiao Jianga et al. found that pterostilbene antagonized homocysteine-induced apoptosis, oxidative stress, and lipid deposition in vascular ECs, an effect proposed to be mediated via the PI3K/Akt/P53 pathway [60]. UNC5B overexpression has been shown to promote intracellular ROS production and activate the P53 pathway, while inhibiting ECs migration and tube formation, ultimately interfering with ECs function [61]. Additionally, in the experimental model of traumatic brain injury (TBI), P53, as a gene related to cell death induction, magnesium treatment reduces the expression of P53 mRNA in the rat cortex induced by traumatic brain injury [62]. In this study, Fig. 5 demonstrates that bioactive glass 1393 promotes wound healing by reducing oxidative stress levels and inhibiting P53 expression on ECs. To further investigate the influence of P53 on wound healing, the present study employed Nutlin-3a as a P53 activator. Treatment with Nutlin-3a has been shown to increase P53 levels, induce conformational changes in Bax, and promote apoptosis in cells with wild-type P53 [37]. According to reports, treating with a small molecule inhibitor of MDM2 Nutlin-3a could augment IR-induced tumor cell elimination and senescence by stabilizing the activation of the P53–P21 signaling pathway [36]. Toru Hashimoto et al. found that after surgery for vascular injury, a micro-osmotic pump was inserted into the abdominal cavity to deliver Nutarin-3a (5 mg $kg^{-1} \cdot day^{-1}$), which up-regulated P53 and its downstream target P21, inhibiting the proliferation and migration of vascular smooth muscle cells (VSMCs) [38]. The results depicted in Fig. 6 showcased the inhibitory effect of P53 activator on vascular growth factor expression, highlighting the critical role of P53 in wound healing. Downstream signals of P53 were also investigated to assess how they affect ECs behavior. During wound healing, matrix metalloproteinases (MMPs) play a vital role in the removal of necrotic tissue by degrading the extracellular matrix, which promotes the migration and proliferation of ECs, leading to increased expression of VEGF and ultimately affecting neovascularization [63]. Deficiencies in MMP9 have been shown to impede vascular neogenesis, resulting in delayed wound healing, impaired keratinocyte migration, and disrupted collagen fiber formation [64]. Elmetwalli et al. have reported the discovery of an anticancer drug that targets the P53/MMP9 axis of action [65]. The P53/MMP9 axis drove MMP9-mediated melanocyte migration, leading to improved pigmentation in vitiligo patients, as reported by Mengyun Su et al. [66]. Taken together, it was found that bioactive glass 1393 regulated the ROS/P53/MMP9 signaling pathway, which increases the expression of angiogenic factors such as eNOS and VEGF, and that the P53 activator Nutlin-3a could inhibit the protective effect of bioactive glass 1393.

Previous research has demonstrated that bioactive glass impacts the proliferation and migration of ECs, which play a crucial role in blood vessels [67,68]. Additionally, LPS can induce cellular oxidative stress [69,70]. Specifically, studies have shown that when bioactive glass 1393 and 45S5 powder are directly added to cell culture, bioactive glass 1393 group exhibits significantly higher metabolic activity compared to bioactive glass 45S5 group. Furthermore, compared with the bioactive glass 45S5 group, the number of cells in the bioactive glass 1393 group is notably greater at the same particle concentration. Quantitative analysis of cell area showed that the coverage area of hMSCs in the bioactive glass 1393 group was significantly greater than that in the bioactive glass 45S5 group [6]. To better simulate *in vivo* experiments, we diluted bioactive glass 1393 powder and added it directly to the ECs culture. Research has shown that bioactive glass 1393 up-regulates the expression of angiogenic-related proteins in ECs. This protects against LPS-induced ECs damage through the ROS/P53/MMP9 signaling pathway, which is consistent with *in vivo* experimental results (Fig. 7). Therefore, cell experiments further support our hypothesis.

Although we found that the direct application of bioactive glass 1393 powder to the wound site improved the rate of wound healing, it remains challenging to determine the exact ionic concentration of bioactive glass within the wound area. Further investigations can be conducted to explore the dosage-dependent impacts of ions on cellular behavior and to establish the

correlation between these effects and the release of ions from bioactive glass particles. Additionally, it is important to examine the influence of the structure of bioactive glass on wound healing. Furthermore, it is worth investigating the potential of utilizing bioactive glass 1393 in the treatment of challenging wounds, such as burns, diabetic ulcers, and infected wounds.

5. Conclusion

In this study, bioactive glass 1393 was synthesized by incorporating additional metallic elements into the traditional bioactive glass (45S5) composition. The results of this study demonstrate that bioactive glass 1393 can induce the release of vascular growth factors and promote angiogenesis by modulating the ROS/P53/MMP9 signaling pathway, ultimately accelerating wound healing. In conclusion, bioactive glass 1393 exhibits significant potential in promoting wound healing and serves as an excellent candidate for future biomedical applications as a biomaterial.

Ethics statement

Animal experimental procedures were approved by the Laboratory Animal Management and Ethics Committee of Wenzhou University. (Ethics approval number: WZU-2022-020).

Data availability

Data will be made available on request.

Author contributions

Xuenan Chen: Investigation, Methodology, Data curation, Formal analysis, Writing-original draft. **Xinyu Ran**: Investigation, Writing-original draft, Writing-review & editing. **Xuebo Wei**: Investigation, Methodology. **Shaodong Chen**: Investigation, Funding acquisition. **Lifei Zhu**: Investigation. **Zhiyong Liao**: Investigation, Funding acquisition. **Ke Xu**: Conceptualization, Supervision, Methodology, Validation, Writing-review. **Weidong Xia**: Investigation.

Declaration of competing interest

The authors declare that they have no known competing financial interests or personal relationships that could have appeared to influence the work reported in this paper.

Acknowledgements

This study was jointly supported by the Zhejiang Provincial Natural Science Foundation of China (LQ23H110002), Ningbo Key Research and Development Program (No. 2022Z146), Lishui Science and Technology Plan Project (2022GYX30), Wenzhou Science and Technology Innovation Project (ZY2020023 and ZY2020026).

References

[1] Brauer DS. Bioactive glasses—structure and properties. Angewandte Chemie International Edition 2015;54(14):4160–81. https://doi.org/10.1002/anie.201405310.
[2] Jones JR. Reprint of: review of bioactive glass: from Hench to hybrids. Acta Biomaterialia 2015;23:S53–82. https://doi.org/10.1016/j.actbio.2015.07.019.
[3] Kargozar S, Baino F, Hamzehlou S, Hill RG, Mozafari M. Bioactive glasses entering the mainstream. Drug Discovery Today 2018;23(10):1700–4. https://doi.org/10.1016/j.drudis.2018.05.027.
[4] Rahaman MN, Day DE, Sonny Bal B, Fu Q, Jung SB, Bonewald LF, et al. Bioactive glass in tissue engineering. Acta Biomaterialia 2011;7(6):2355–73. https://doi.org/10.1016/j.actbio.2011.03.016.
[5] Zhang K, Chai B, Ji H, Chen l, Ma Y, Zhu L, et al. Bioglass promotes wound healing by inhibiting endothelial cell pyroptosis through regulation of the connexin 43/reactive oxygen species (ROS) signaling pathway. Laboratory Investigation 2022;102(1):90–101. https://doi.org/10.1038/s41374-021-00675-6.
[6] Qazi TH, Hafeez S, Schmidt J, Duda GN, Boccaccini AR, Lippens E. Comparison of the effects of 45S5 and 1393 bioactive glass microparticles on hMSC behavior. Journal of Biomedical Materials Research Part A 2017;105(10):2772–82. https://doi.org/10.1002/jbm.a.36131.
[7] Nakiou EA, Lazaridou M, Pouroutzidou GK, Michopoulou A, Tsamesidis I, Liverani L, et al. Poly(Glycerol succinate) as coating material for 1393 bioactive glass porous scaffolds for tissue engineering applications. Polymers 2022;14(22). https://doi.org/10.3390/polym14225028.
[8] Kunisch E, Fiehn L, Saur M, Arango-Ospina M, Merle C, Hagmann S, et al. A comparative in vitro and in vivo analysis of the biological properties of the 45S5-, 1393-, and 0106-B1-bioactive glass compositions using human bone marrow-derived stromal cells and a rodent critical size femoral defect model. Biomaterials advances 2023;153:213521. https://doi.org/10.1016/j.bioadv.2023.213521.
[9] Wei X, Liao Z, Yang L, Wu F, Chen S, Shao C, et al. Phosphorus magnesium fiber regulates macrophage polarization through TRPM7 to accelerate wound healing. Applied Materials Today 2023;31:101758. https://doi.org/10.1016/j.apmt.2023.101758.
[10] Gupta S, Prasad P, Roy A, Alam MM, Ahmed I, Bit A. Metallic ion-based graphene oxide functionalized silk fibroin-based dressing promotes wound healing via improved bactericidal outcomes and faster re-epithelization. Biomedical Materials 2022;17(3):035010. https://doi.org/10.1088/1748-605X/ac64dd.
[11] Ding Chen ZL, Su Zhikang, Huang Jiangyong, Pi Yixing, Ouyang Yuanting, Luo Tao, et al. Selenium-doped mesoporous bioactive glass regulates macrophage metabolism and polarization by scavenging ROS and promotes bone regeneration in vivo. ACS Appl Mater Interfaces 2023. https://doi.org/10.1021/acsami.3c03446.
[12] Zhu C, Cao R, Zhang Y, Chen R. Metallic ions encapsulated in electrospun nanofiber for antibacterial and angiogenesis function to promote wound repair. Front cell dev biol 2021;9:660571. https://doi.org/10.3389/fcell.2021.660571.
[13] Gupta S, Dutta P, Acharya V, Prasad P, Roy A, Bit A. Accelerating skin barrier repair using novel bioactive magnesium-doped nanofibers of non-mulberry silk fibroin during wound healing. Journal of Bioactive Compatible Polymers 2021;37(1):38–52. https://doi.org/10.1177/08839115211061737.
[14] Fraisl P, Mazzone M, Schmidt T, Carmeliet P. Regulation of angiogenesis by oxygen and metabolism. Developmental Cell 2009;16(2):167–79. https://doi.org/10.1016/j.devcel.2009.01.003.
[15] Moreira HR, Marques AP. Vascularization in skin wound healing: where do we stand and where do we go? Current Opinion in Biotechnology 2022;73:253–62. https://doi.org/10.1016/j.copbio.2021.08.019.
[16] Han X, Chen S, Cai Z, Zhu Y, Yi W, Guan M, et al. A diagnostic and therapeutic hydrogel to promote vascularization via blood sugar reduction for wound healing. Advanced Functional Materials 2023;33(14):2213008. https://doi.org/10.1002/adfm.202213008.
[17] Wen W, Yang L, Wang X, Zhang H, Wu F, Xu K, et al. Fucoidan promotes angiogenesis and accelerates wound healing through AKT/Nrf2/HIF-1α signalling pathway. International Wound Journal 2023. https://doi.org/10.1111/iwj.14239.
[18] Carmeliet P, Jain RK. Angiogenesis in cancer and other diseases. Nature 2000;407(6801):249–57. https://doi.org/10.1038/35025220.
[19] Chen L, Hao L, Yanshuo C, FangFang W, Daqin C, Weidong X, et al. Grape seed proanthocyanidins regulate mitophagy of endothelial cells and promote wound healing in mice through p-JNK/FOXO3a/ROS signal pathway. Arch Biochem Biophys 2023;749. https://doi.org/10.1016/j.abb.2023.109790.
[20] Bouloumié A, Schini-Kerth VB, Busse R. Vascular endothelial growth factor up-regulates nitric oxide synthase expression in endothelial cells1. Cardiovascular Research 1999;41(3):773–80. https://doi.org/10.1016/s0008-6363(98)00228-4.
[21] Du X, Ou X, Song T, Zhang W, Cong F, Zhang S, et al. Adenosine A2B receptor stimulates angiogenesis by inducing VEGF and eNOS in human microvascular endothelial cells. Exp Biol Med 2015;240(11):1472–9. https://doi.org/10.1177/1535370215584939.
[22] Thibeault S, Rautureau Y, Oubaha M, Faubert D, Wilkes BC, Delisle C, et al. S-nitrosylation of β-catenin by eNOS-derived NO promotes VEGF-induced endothelial cell permeability. Molecular cell 2010;39(3):468–76.
[23] Bi L, Jung S, Day D, Neidig K, Dusevich V, Eick D, et al. Evaluation of bone regeneration, angiogenesis, and hydroxyapatite conversion in critical-sized rat calvarial defects implanted with bioactive glass scaffolds. Journal of Biomedical Materials Research Part A 2012;100A(12):3267–75. https://doi.org/10.1002/jbm.a.34272.
[24] Bi L, Rahaman MN, Day DE, Brown Z, Samujh C, Liu X, et al. Effect of bioactive borate glass microstructure on bone regeneration, angiogenesis, and hydroxyapatite conversion in a rat calvarial defect model. Acta Biomaterialia 2013;9(8):8015–26. https://doi.org/10.1016/j.actbio.2013.04.043.
[25] Deng L, Du C, Song P, Chen T, Rui S, Armstrong DG, et al. The role of oxidative stress and antioxidants in diabetic wound healing. Oxid Med Cell Longev 2021;2021:8852759. https://doi.org/10.1155/2021/8852759.

[26] Xu Z, Liu Y, Ma R, Chen J, Qiu J, Du S, et al. Thermosensitive hydrogel incorporating prussian blue nanoparticles promotes diabetic wound healing via ROS scavenging and mitochondrial function restoration. ACS Appl Mater Interfaces 2022;14(12):14059–71. https://doi.org/10.1021/acsami.1c24569.
[27] Qin Y, Wu K, Zhang Z, Pan R, Lin Z, Zhang W, et al. NLRC3 deficiency promotes cutaneous wound healing due to the inhibition of p53 signaling. Biochimica et Biophysica Acta (BBA) - Molecular Basis of Disease 2022;1868(11). https://doi.org/10.1016/j.bbadis.2022.166518.
[28] Zhang C, Li Z, Wang J, Jiang X, Xia M, Wang J, et al. Ethanol extracts of solanum lyratum thunb regulate ovarian cancer cell proliferation, apoptosis, and epithelial-to-mesenchymal transition (EMT) via the ROS-mediated p53 pathway. Journal of Immunology Research 2021;2021:1–16. https://doi.org/10.1155/2021/5569354.
[29] Das B, Sahoo S, Mallick B. HIWI2 induces G2/M cell cycle arrest and apoptosis in human fibrosarcoma via the ROS/DNA damage/p53 axis. Life Sciences 2022;293. https://doi.org/10.1016/j.lfs.2022.120353.
[30] Wang L, Zhang ZG, Zhang RL, Gregg SR, Hozeska-Solgot A, LeTourneau Y, et al. Matrix metalloproteinase 2 (MMP2) and MMP9 secreted by erythropoietin-activated endothelial cells promote neural progenitor cell migration. The Journal of Neuroscience 2006;26(22):5996–6003. https://doi.org/10.1523/jneurosci.5380-05.2006.
[31] Park SY, Jung CH, Song B, Park OJ, Kim Y-M. Pro-apoptotic and migration-suppressing potential of EGCG, and the involvement of AMPK in the p53-mediated modulation of VEGF and MMP-9 expression. Oncology Letters 2013;6(5):1346–50. https://doi.org/10.3892/ol.2013.1533.
[32] Hoppe A, Jokic B, Janackovic D, Fey T, Greil P, Romeis S, et al. Cobalt-releasing 1393 bioactive glass-derived scaffolds for bone tissue engineering applications. ACS Appl Mater Interfaces 2014;6(4):2865–77. https://doi.org/10.1021/am405354y.
[33] Wu J, Chen A, Zhou Y, Zheng S, Yang Y, An Y, et al. Novel HS-Releasing hydrogel for wound repair via in situ polarization of M2 macrophages. Biomaterials 2019;222:119398. https://doi.org/10.1016/j.biomaterials.2019.119398.
[34] Hosgood G. Stages of wound healing and their clinical relevance. Veterinary Clinics: Small Animal Practice 2006;36(4):667–85.
[35] Roy S, Santra S, Das A, Dixith S, Sinha M, Ghatak S, et al. Staphylococcus aureus biofilm infection compromises wound healing by causing deficiencies in granulation tissue collagen. Annals of surgery 2020;271(6):1174.
[36] Luo H, Yount C, Lang H, Yang A, Riemer EC, Lyons K, et al. Activation of p53 with Nutlin-3a radiosensitizes lung cancer cells via enhancing radiation-induced premature senescence. Lung cancer 2013;81(2):167–73.
[37] Kojima K, Konopleva M, Samudio IJ, Shikami M, Cabreira-Hansen M, McQueen T, et al. MDM2 antagonists induce p53-dependent apoptosis in AML: implications for leukemia therapy. Blood 2005;106(9):3150–9.
[38] Hashimoto T, Ichiki T, Ikeda J, Narabayashi E, Matsuura H, Miyazaki R, et al. Inhibition of MDM2 attenuates neointimal hyperplasia via suppression of vascular proliferation and inflammation. Cardiovascular research 2011;91(4):711–9.
[39] Xu Q, Zheng Z, Wang B, Mao H, Yan F. Zinc ion coordinated poly (ionic liquid) antimicrobial membranes for wound healing. ACS Appl Mater Interfaces 2017;9(17):14656–64.
[40] Silver S, Phung LT, Silver G. Silver as biocides in burn and wound dressings and bacterial resistance to silver compounds. J Ind Microbiol Biotechnol 2006;33(7):627–34.
[41] Zhang Z, Li W, Liu Y, Yang Z, Ma L, Zhuang H, et al. Design of a biofluid-absorbing bioactive sandwich-structured Zn–Si bioceramic composite wound dressing for hair follicle regeneration and skin burn wound healing. Bioactive Materials 2021;6(7):1910–20. https://doi.org/10.1016/j.bioactmat.2020.12.006.
[42] Zhang Z, Zhang Y, Li W, Ma L, Wang E, Xing M, et al. Curcumin/Fe-SiO2 nano composites with multi-synergistic effects for scar inhibition and hair follicle regeneration during burn wound healing. Applied Materials Today 2021;23:101065.
[43] Zhang Z, Dai Q, Zhang Y, Zhuang H, Wang E, Xu Q, et al. Design of a multi-functional biomaterial inspired by ancient Chinese medicine for hair regeneration in burned skin. ACS Appl Mater Interfaces 2020;12(11):12489–99.
[44] Eming SA, Brachvogel B, Odorisio T, Koch M. Regulation of angiogenesis: wound healing as a model. Prog Histochem Cytochem 2007;42(3):115–70.
[45] Matsuo R, Kishibe M, Horiuchi K, Kano K, Tatsukawa T, Hayasaka T, et al. Ninjurin1 deletion in NG2-positive pericytes prevents microvessel maturation and delays wound healing. JID Innovations 2022;2(6):100141. https://doi.org/10.1016/j.xjidi.2022.100141.
[46] Chekenya M, Hjelstuen M, Enger PØ, Thorsen F, Jacob AL, Probst B, et al. NG2 proteoglycan promotes angiogenesis-dependent tumor growth in the central nervous system by sequestering angiostatin. The FASEB Journal 2002;16(6):586–8.
[47] Fukushi J-i, Makagiansar IT, Stallcup WB. NG2 proteoglycan promotes endothelial cell motility and angiogenesis via engagement of galectin-3 and α3β1 integrin. Molecular biology of the cell 2004;15(8):3580–90.
[48] Hesp ZC, Yoseph RY, Suzuki R, Jukkola P, Wilson C, Nishiyama A, et al. Proliferating NG2-cell-dependent angiogenesis and scar formation alter axon growth and functional recovery after spinal cord injury in mice. Journal of Neuroscience 2018;38(6):1366–82.
[49] Ozerdem U, Stallcup WB. Pathological angiogenesis is reduced by targeting pericytes via the NG2 proteoglycan. Angiogenesis 2004;7:269–76.
[50] Kroll J, Waltenberger J. VEGF-A induces expression of eNOS and iNOS in endothelial cells via VEGF receptor-2 (KDR). Biochem Biophys Res Commun 1998;252(3):743–6.
[51] Suganthalakshmi B, Anand R, Kim R, Mahalakshmi R, Karthikprakash S, Namperumalsamy P, et al. Association of VEGF and eNOS gene polymorphisms in type 2 diabetic retinopathy. Mol Vis 2006;12(1):336–41.
[52] Gentile C, Muise-Helmericks RC, Drake CJ. VEGF-mediated phosphorylation of eNOS regulates angioblast and embryonic endothelial cell proliferation. Developmental Biology 2013;373(1):163–75. https://doi.org/10.1016/j.ydbio.2012.10.020.
[53] Li Y, Zhao Y-J, Zou Q-Y, Zhang K, Wu Y-M, Zhou C, et al. Preeclampsia does not alter vascular growth and expression of CD31 and vascular endothelial cadherin in human placentas. J Histochem Cytochem 2015;63(1):22–31.
[54] Vailhé B, Arck P, Kapp M, Dietl J. Human first-trimester decidua vascular density: an immunohistochemical study using VE-cadherin and endoglin as endothelial cell markers. American Journal of Reproductive Immunology 2000;44(1):9–15.
[55] Wyder L, Vitaliti A, Schneider H, Hebbard LW, Moritz DR, Wittmer M, et al. Increased expression of H/T-cadherin in tumor-penetrating blood vessels. Cancer research 2000;60(17):4682–8.
[56] Tsuneki M, Madri JA. CD44 regulation of endothelial cell proliferation and apoptosis via modulation of CD31 and VE-cadherin expression. Journal of Biological Chemistry 2014;289(9):5357–70.
[57] Azzouz D, Khan MA, Palaniyar N. ROS induces NETosis by oxidizing DNA and initiating DNA repair. Cell Death Discovery 2021;7(1):113.
[58] Juan CA, Pérez de la Lastra JM, Plou FJ, Pérez-Lebeña E. The chemistry of reactive oxygen species (ROS) revisited: outlining their role in biological macromolecules (DNA, lipids and proteins) and induced pathologies. International Journal of Molecular Sciences 2021;22(9):4642.
[59] Srinivas US, Tan BW, Vellayappan BA, Jeyasekharan AD. ROS and the DNA damage response in cancer. Redox biology 2019;25:101084.
[60] Jiang Q, Wang L, Si X, Bian Y, Zhang W, Cui H, et al. Pterostilbene antagonizes homocysteine-induced oxidative stress, apoptosis and lipid deposition in vascular endothelial cells. Food Science Human Wellness 2023;12(5):1683–92.
[61] Yang Z, Li H, Luo P, Yan D, Yang N, Zhang Y, et al. UNC5B promotes vascular endothelial cell senescence via the ROS-mediated P53 pathway. Oxid Med Cell Longev 2021;2021:1–13. https://doi.org/10.1155/2021/5546711.
[62] Muir JK, Raghupathi R, Emery DL, Bareyre FM, McIntosh TK. Postinjury magnesium treatment attenuates traumatic brain injury-induced cortical induction of p53 mRNA in rats. Experimental neurology 1999;159(2):584–93.
[63] Franchi A, Santucci M, Masini E, Sardi I, Paglierani M, Gallo O. Expression of matrix metalloproteinase 1, matrix metalloproteinase 2, and matrix metalloproteinase 9 in carcinoma of the head and neck. Cancer 2002;95(9):1902–10. https://doi.org/10.1002/cncr.10916.
[64] Cho H, Balaji S, Hone NL, Moles CM, Sheikh AQ, Crombleholme TM, et al. Diabetic wound healing in a MMP9-/- mouse model. Wound Repair Regen 2016;24(5):829–40. https://doi.org/10.1111/wrr.12453.
[65] Elmetwalli A, Diab T, Albalawi AN, El-Naggar SA, El-Far AH, Ghedan AR, et al. Diarylheptanoids/sorafenib as a potential anticancer combination against hepatocellular carcinoma: the p53/MMP9 axis of action. Naunyn-Schmiedeberg's Archives of Pharmacology 2023;396(10):2501–17. https://doi.org/10.1007/s00210-023-02470-0.
[66] Su M, Miao F, Jiang S, Shi Y, Luo L, He X, et al. Role of the p53-TRPM1/miR-211-MMP9 axis in UVB-induced human melanocyte migration and its potential in repigmentation. Int J Mol Med 2020;45(4):1017–26. https://doi.org/10.3892/ijmm.2020.4478.
[67] Li H, He J, Yu H, Green CR, Chang J. Bioglass promotes wound healing by affecting gap junction connexin 43 mediated endothelial cell behavior. Biomaterials 2016;84:64–75.
[68] Mao C, Chen X, Miao G, Lin C. Angiogenesis stimulated by novel nanoscale bioactive glasses. Biomedical materials 2015;10(2):025005.
[69] Noworyta-Sokołowska K, Górska A, Gołembiowska K. LPS-induced oxidative stress and inflammatory reaction in the rat striatum. Pharmacological reports 2013;65(4):863–9.
[70] Sul O-J, Ra SW. Quercetin prevents LPS-induced oxidative stress and inflammation by modulating NOX2/ROS/NF-kB in lung epithelial cells. Molecules 2021;26(22):6949.